Tribol Lett (2017) 65:5
DOI 10.1007/s11249-016-0785-5

ORIGINAL PAPER

Elastic Waves of a Single Elasto-Hydrodynamically Lubricated Contact

S. Schnabel[1] · P. Marklund[2] · R. Larsson[2]

Received: 9 August 2016 / Accepted: 7 November 2016 / Published online: 19 November 2016

Abstract Elastic waves are widely used for condition monitoring of rolling element bearings through vibration or acoustic emission measurements. While vibration signals are understood to a high degree due to many scientific investigations as well as a long history of usage in the field, acoustic emission signals of rolling element bearings are poorly understood. Therefore, this investigation presents simulation studies and measurements of a single elasto-hydrodynamically lubricated (EHL) contact. In this investigation the EHL contact is a ball bouncing on a lubricated plate. The simulation based on Green's function and the measurements based on a accelerometer to some extent agree. A shift of zero frequencies towards higher frequencies when compared to Hertzian reference measurements was determined for an infinite plate setup. Taking boundary restrictions into account, elastic waves of a Hertzian contact and an EHL contact only differ by a damping of higher resonances which is most likely caused by the EHL film.

Keywords EHL contact · EHL · Hertz contact · Elastic waves · Acoustic emission · Green's function · Ball impact · Bouncing ball

List of symbols

c_p, c_{p1}, c_{p2}	Speed of elastic pressure wave and indexes are for lubricant layer (2) and solid plate (1)
$E-1, E_2$	Elastic modulus ball(1), plate(2)
f_j	Force in time domain in direction j
$f_{\max}$	Maximum Hertzian force
$f_{\text{norm},N}$	Normalized zero frequency of N-order
$f_{\text{zero},N}$	Zero frequency of N-order
g_{kj}	Green's function from direction j to k
h_{00}	Initial film thickness
R	Ball radius
RC	Reflection coefficient
t	Time (measurement base)
t_c	Hertzian contact time
t_{film}	Time for ball to penetrate lubricant film
u_k	Displacement in time domain in direction k
v_0	Impact velocity
x	Position of sensor
Z_1, Z_2	Acoustic impedance solid plate(1), lubricant layer/air(2)
δ_1, δ_2	Material factor ball(1), plate(2)
ν_1, ν_2	Poisson's ratio ball(1), plate(2)
ξ	Position of impact
τ	Time (impact base)
ρ_1, ρ_2	Density ball(1), plate(2)

1 Introduction

Acoustic emission (AE) has been shown in several studies to be a viable method for condition monitoring of rolling element bearings. Signals from contaminated bearings were in these studies successfully correlated to type [1, 2], size [1–3] and concentration [1, 2] of particle contamination. In

✉ S. Schnabel
stephan.schnabel@ltu.se

[1] Division of Machine Elements, SKF-University Technology Center, Luleå University of Technology, 97187 Luleå, Sweden

[2] Division of Machine Elements, Luleå University of Technology, 97187 Luleå, Sweden

addition, the type of lubricant [4–6] and the lubrication absence [7] in both contaminated and uncontaminated cases were correlated with signals monitored by acoustic emission transducers. Artificially implemented dents [8] on the outer ring and failure growth [9] was another operating condition with which AE was correlated. In 2014 Hamel et al. [10] determined the relation between acoustic emission signals and the lubrication regime. However, regardless of the application of acoustic emission in scientific studies it is still a rarely used method of condition monitoring in industrial applications. The signal-to-noise ratio (SNR) is one factor. Special test rigs which limit the amount of noise from other machinery parts are employed in all the experiments in the mentioned studies. Additionally, most of them operate in severe operating conditions, which improves the SNR even further, due to a high signal strength. In industrial applications, however, it is more difficult to observe the phenomena presented in the investigations mentioned. For these reasons, it is important to improve signal processing of acoustic emission raw data, and in addition, there is a need for the origin of acoustic emission in an elasto-hydrodynamic lubricated (EHL) contact to be understood.

One way of improving understanding of the origin of acoustic emission in an EHL contact is to break the rolling element bearing down into the component level (AE signals of transient forces, sliding/friction and plasticity). One of these investigations on a component level was carried out by Rahman et al. [11]. Their study focused on the correlation of acoustic emission signal and contact fatigue in a twin-disc setup. A pure sliding EHL contact and its acoustic emission were studied by Wang et al. [12] in a ball on disc apparatus. There are, however, few investigations on a component level. The difficulties of the complex nature of an EHL contact itself remain. This complexity of an EHL contact is also a reason for fundamental research in acoustic emission to focus on fundamental sources such as transient forces [13] or cavitation [14] which both occur in an EHL contact. However, studying fundamental sources is just a first step towards the study of full EHL contacts. Therefore, this article investigates EHL contacts based on the investigations mentioned into transient force and cavitation. In this investigation, a special case of EHL contact, with a bouncing ball on a lubricated plate, is examined. This EHL contact was chosen because transient forces and cavitation can be expected, while sliding as a source of acoustic emission is minimized, due to a pure squeeze contact.

2 Experimental Setup

All experiments were carried out at room temperature and in a laboratory environment. Acoustic emission signals were sampled with a 14-bit digitizer PCI-card of GaGe (product number OSC-432-007). Sample rate and total sample length were set to 10MSamples/s and 10.000 Samples, respectively. Additionally, to the sample length a pre-trigger of 10 Samples was used which equivalent to 1 µs. This short pre-trigger could be used due to the low noise level and the low trigger threshold. This threshold was −3% of the measurement range which was ±10 V. Signals were triggered on a negative flank. As a comparison, the background noise during experiments was between ±1 and ±2% of the measurement range.

To study an elasto-hydrodynamically lubricated contact, a thin layer of lubricant was applied onto the plates or discs. In theory the layer should be as thick as the maximum film thickness of the EHL contact to avoid viscous damping of the ball impact. In practice, the lubricant layer was applied as thinly as possible, so that viscous damping effects were minimized. In this way, 0.5 ml of lubricant was applied at the position of the ball impact and smeared out across an area of 50 mm × 50 mm. This lubricant layer was then covered with a non-cellulose-based paper, absorbing the majority of the lubricant film. After removing the paper, the film was exposed for 10 min to a low and steady air flow, which distributed the lubrication layer evenly and caused possible air bubbles to burst. This procedure was identical for all applied lubricant films in this investigation.

All ball samples were standard rolling element bearing components and had the tolerance G20. Furthermore were all ball samples of the steel type OVAKO825B. Throughout the investigation, it is further assumed that the pressure wave speed is $5900\frac{m}{s}$ for both plate and discs.

2.1 Infinite Plate

Figure 1 shows a schematic drawing of the experimental setup of tests on a steel plate with the brand name Toolox44 that is considered to have infinite length and breadth. The plate used has the dimensions of 1 × 0.5 × 0.051 m and can be considered infinite for a measurement duration of 84 µs because reflections in horizontal directions are not relevant. The shortest horizontal reflection time (based on width 0.5m) is 84.75 µs which means the elastic wave does not return to the point of measurement within the recorded time. Hence, the plate can be considered infinite and boundaries do not need to be considered in the horizontal direction. However, across the plate (0.051 m) reflection times are shorter and therefore boundaries need to be considered in the vertical direction. Therefore, the plate was boundary restricted in one dimension and infinite in the two horizontal dimensions. Due to the two boundary free dimensions, the plate is considered to be an infinite plate throughout the article.

The plate was, during the experiments, resting on two rubber cylinders (∅10 mm) placed on each end of the 1-m side (Fig. 1). The AE sensor was mounted centred

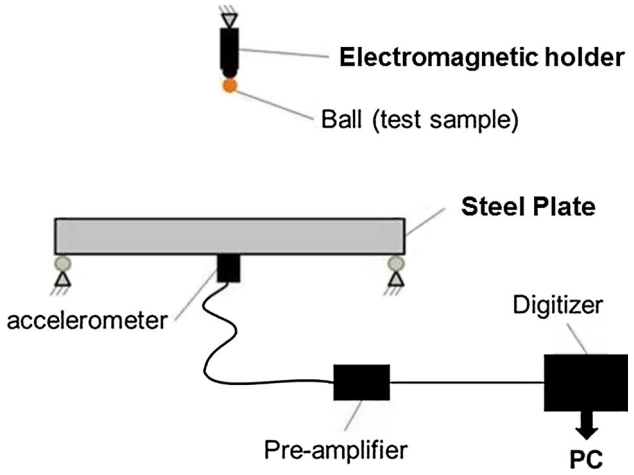

Fig. 1 Schematic drawing of experimental setup for tests on plate considered to be infinite

underneath the plate and was vertically aligned with a magnetic holder. In this way, the ball impact occurred centred on the sensor position only separated vertically by the plate thickness (epicentral setup). To improve the accuracy of the impact position, the magnetic holder was shaped as a sphere to obtain automatic alignment based on gravity.

Acoustic emission signals were recorded by a broadband flat-response transducer (WSα) from Physical Acoustics in combination with a preamplifier (Physical Acoustic 2/4/6C). The sensor head of this sensor has a diameter of 19 mm. In addition to the amplifying circuit, the amplifier had an inbuilt bandpass filter with corner frequencies of 100 kHz and 1.2 MHz. In all experiments presented in this article, the AE sensor was attached with beeswax to the specimens. Therefore, a small amount of beeswax was applied onto the plate and heated to 75 °C, followed by pressing the AE sensor with dead weight onto the plate. Before starting the tests, a temperature measurement made certain that the plate was cooled to below 25 °C. All signals of the acoustic emission sensor presented in this investigation were compensated for the sensor function. This sensor function was obtained by a glass capillary burst experiment as suggested by McLaskey and Glaser [15] as a method for absolute calibration.

For experiments with the infinite plate setup, four different steel balls were used and each ball was dropped from three different heights (Table 1). Balls were released by a magnetic holder. This holder consists of a coil and a iron cylinder, which is partly insert into the coil. The cylinder has additionally the shape of a half sphere at one side. This half-spherical shape limits the contact area between holder and the ball to release, allowing a clean release without deflection. The penetration depth of the coil and the current were adjusted for each ball size to minimize the magnetic forces to a minimum, but still large enough to overcome gravity. Each combination (ball size and height) was repeated 8 times for the lubricated experiments. Hertzian reference measurements under dry conditions were repeated 4 times for each combination.

Table 1 Test setup for infinite plate case

Ball samples	Ball radius (mm)	Drop heights (mm)
RB1.5 G20	0.75	350
RB2 G20	1.0	250
RB3 G20	1.5	150
RB4 G20	2.0	

2.2 Boundary Restricted Systems

Tests for boundary restricted systems were executed on disc samples with a diameter of 103.8 mm. The disc samples only differed in height (Table 2). In this investigation, all disc materials were Steel2511. Due to the dimensions of the disc, reflection cannot be neglected and boundaries of all dimensions need to be considered. Therefore, the term boundary restricted system will be used for all experiments with discs. The balls were for the boundary restricted cases dropped from three different heights onto the discs. As previously shown [16], there are in boundary restricted systems two major cases; one where the exciting source and elastic wave are independent, and one where both interact with each other. The latter case (interaction between source and wave) is studied in this article for an EHL contact. The laser doppler vibrometer (LDV) used for acoustic emission measurement in the boundary restricted system is the Polytec OFV056. The Polytec OFV056 was used in combination with a control and preamplifying unit of the same manufacturer (Polytec OFV3001S). As shown in Fig. 2, the laser had to be redirected, which was done by an optical mirror (Thorlabs PF20-03-P01).

$$\begin{aligned} f(\tau) &= f_{\max}\sin\left(\frac{\pi(\tau - t_{\text{film}})}{t_c}\right)^{3/2}, \quad t_{\text{film}} \le \tau \le (t_c + t_{\text{film}}) \\ f(\tau) &= 0, \qquad \tau < t_{\text{film}} f(\tau) \\ f(\tau) &= 0, \qquad \tau > (t_c + t_{\text{film}}) \end{aligned} \tag{1}$$

The sensitivity setting was chosen to be 1.25 mm/s, which resulted in a frequency range of 1 Hz to 1 MHz of the LDV system. As for the infinite plate setup, the measurement point and impact point were vertically aligned to measure an epicentral impact. The magnetic holder and sampling card were also identical in both measurement setups.

Table 2 Test setup for boundary restricted case

Ball samples	Ball radius (mm)	Drop heights (mm)	Disc heights (mm)
RB2 G20	1.0	350	5
RB3 G20	1.5	250	7
RB4 G20	2.0	150	
RB6 G20	3.0		
RB8 G20	4.0		

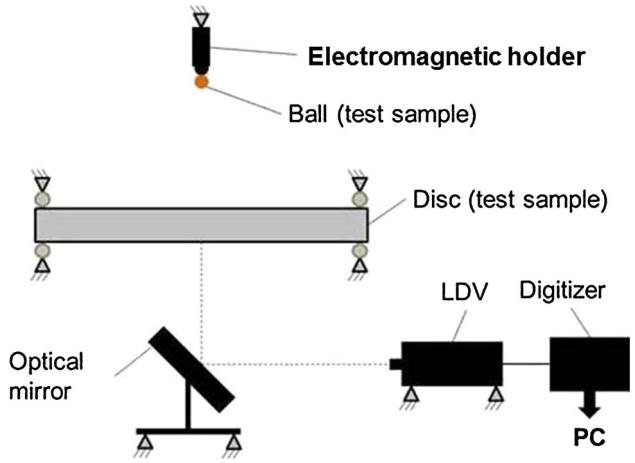

Fig. 2 Schematic drawing of the experimental setup for tests on boundary restricted systems

However, the setups differ in terms of positioning of the plates and discs, respectively. While the plate was resting on rubber cylinders (Fig. 1), the discs needed to be clamped in between two rubber seals (Fig. 2), because the net weight of the discs was not enough to prohibit movement during impacts. The dimension of the rubber seals was ∅100 mm and the thickness was ∅2.5 mm. For the boundary restricted systems, both EHL contact and reference measurements with Hertzian contacts were repeated 8 times for each combination (ball size, disc height and drop height).

3 Theory for Simulation

Signals presented in this investigation are simulated based on a Green's function approach (2), where force function ($f_j(\xi,\tau)$) and Green's function ($g_{kj}(x,t,\xi,\tau)$) are convolved with each other to obtain a time signal for the displacement ($u_k(x,t)$). Variables x, t, ξ and τ represent thereby the position of the sensor, the time scale of the sensor signal, the position of the impact and the time scale of the impact, respectively. Indexes indicate the direction of the force, displacement and Green's function.

$$u_k(x,t) = f_j(\xi,\tau) * g_{kj}(x,t,\xi,\tau) \tag{2}$$

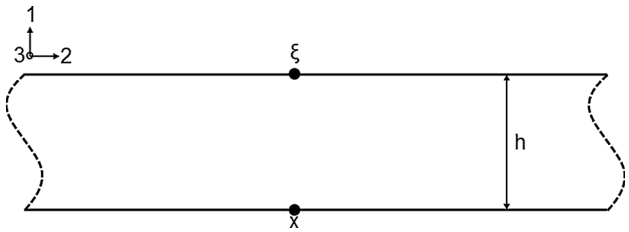

Fig. 3 Schematic drawing for declaration of experimental setup

As Fig. 3 shows, index 1 refers to the direction perpendicular to the plate. It is assumed for the entire article that displacements ($u_k(x,t)$) and all initiating forces ($f_j(\xi,\tau)$) are perpendicular to the plate, which results in $k = j = 1$ for indexes of Eq. (2).Green's function for an infinite plate was calculated numerically by using Hsu's script [17], which is valid for the infinite plate setup and a measurement time of 84 µs. The force function, however, was calculated either numerically or analytically for EHL impacts and Hertzian impacts, respectively. Forces of EHL impacts are calculated by using a numerical EHL solver of Larsson and Höglund [18]. The script requires an initial film thickness (h_{00}) as an input parameter. This initial film thickness needs to be minimal to minimize viscous damping of the ball by the lubricant film. However, the film thickness needs to be at least as thick as the maximum film thickness of the EHL contact. After empirical trials, the factor for the initial film thickness (h_{00}) was set to 10 µm and was identical for all simulations in this investigation.

In the case of Hertzian impacts, a modified version of Reed's [19] elastic contact model was employed (Eq. (1)). Maximum force ($f_{\max}$) and contact time (t_c) are calculated according to the following equations:

$$f_{\max} = 1.917\rho_1^{3/5}(\delta_1+\delta_2)^{-2/5}R_1^2 v_0^{6/5} \tag{3}$$

$$t_c = 4.53(4\rho_1\pi(\delta_1+\delta_2)/3)^{2/5}R_1 v_0^{-1/5} \tag{4}$$

where $\delta_i = \frac{1-\nu_i^2}{\pi E_i}$ and indexes 1 and 2 refer to ball and plate, respectively, while the film offset time (t_{film}) is the time required to pass an initial film:

$$t_{\text{film}} = \frac{h_{00}}{v_0} \tag{5}$$

While the ball needs to pass the initial film thickness in the EHL model, Reed's original equation does not take that into account and starts from $t = 0$. To synchronize both force functions with respect to the initial metal to metal contact, Reed's force function was shifted. This shift was done by implementing an additional variable, the film offset time (t_{film}).

4 Results and Discussion

This section is divided into two parts, based on the separation mentioned in the experimental setup section. In the first part, results of elastic waves without restriction caused by an EHL impact will be presented using a infinite plate setup. The second part includes results on the resonance excitation of EHL impacts in boundary restricted systems. Please notice all signals from the infinite plate are recorded with an AE sensor, while for the boundary restricted systems (small discs) a laser doppler vibrometer (LDV) was used.

4.1 Infinite Plate

In Fig. 4 forces are generated in both a dry and a lubricated contact for an impact of a ball (RB2 G20) from a height of 350 mm. Differences in contact time, as well as amplitude, are observed. The EHL force reaches its maximum earlier than the Hertzian force function, which is in line with the investigation of Larsson and Höglund [18]. Therefore, the force functions are considered to be evaluated and are the main input for simulations presented in this investigation.

Results of simulated signals based on the force functions show decreased zero frequencies due to the increased contact time for EHL contacts and additional excitation of

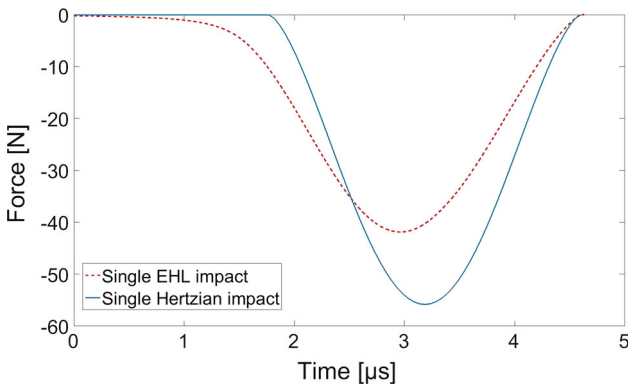

Fig. 4 Simulated and calculated force caused by an EHL and a Hertzian impact, respectively

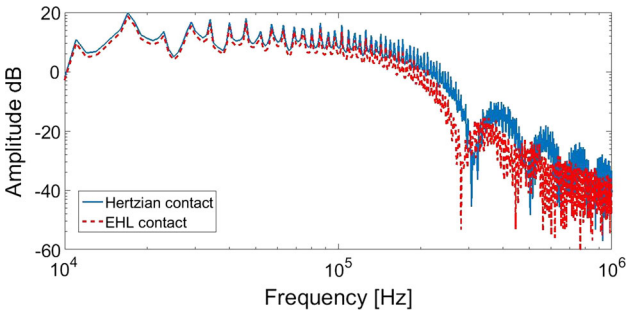

Fig. 5 Spectra of simulated signals of Hertzian and EHL impacts with a ball (RB2 G20) dropped from 350 mm height. Simulation based on Eq. (2) (Color figure online)

higher frequencies (Fig. 5). The blue solid line represents the spectra of an impact of a ball (RB2 G20) dropped from a height of 350 mm. The spectra show distinct frequency minimums (zero frequencies, $f_{\text{Zero},N}$) based on the contact time of the Hertzian contact as shown by McLaskey and Glaser [13]:

$$f_{\text{zero},N} = \frac{0.75 + N}{t_c} \tag{6}$$

$$f_{\text{norm},N} = f_{\text{zero},N} * t_c \tag{7}$$

The red dashed line shows the spectra of the simulated EHL impact. Comparing the spectra to the Hertzian impact shows zero frequencies shift towards lower frequencies. Using Eq. (7) gives indication of expected positions of frequency minimums. While Hertzian zero frequencies agree with McLaskey's and Glaser's [13] suggested positions ($f_{\text{norm},N} = [1.75, 2.75, 3.75]$), zero frequencies for EHL impacts shift according to the simulation to 1.61 and 2.53. The third zero frequency cannot be identified, which can be a result of several causes, such as cavitation, signal-to-noise ratio or an uncertain defined contact time. Even though Zong et al. [14] demonstrate cavitation excites high frequencies, which would be in line with covering zero frequencies such as in this case for third order and higher orders, the uncertain defined contact time in the EHL case is the most plausible explanation for the covering of the zero frequencies of third order and higher, which is observed in both simulation and measurement. Signal-to-noise ratio can be eliminated, due to the fact that covering of the zero frequencies of third and higher order is present in the simulations.

Figure 6 shows the comparison of simulation (blue dashed line) and measured (yellow solid line) signals for a Hertzian impact. As an earlier investigation [13] showed, agreement is good and could be replicated for this investigation. This demonstrates that Hertzian measurement is a good reference measurement. A slight overestimation of the simulated signal can be seen, which is especially interesting if compared to Fig. 7 (comparison of EHL

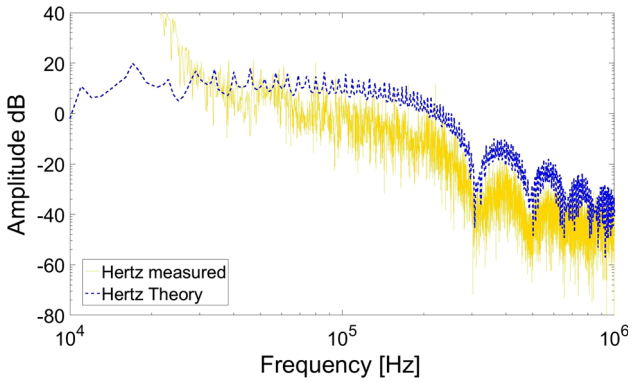

Fig. 6 Comparison of simulated and measured spectra of Hertzian impacts with a ball (RB2 G20) dropped from 350 mm height (Color figure online)

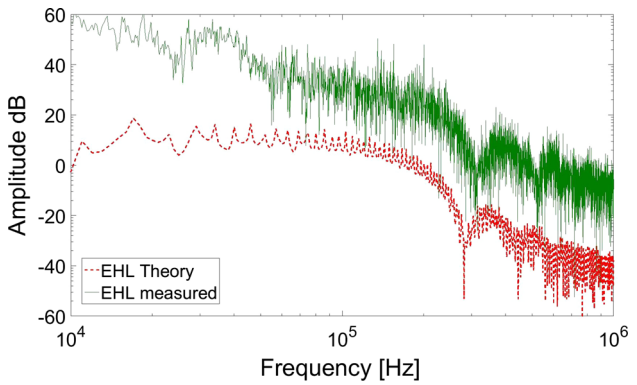

Fig. 7 Comparison of simulated and measured spectra of EHL impacts with a ball (RB2 G20) dropped from 350 mm height

impacts). For EHL impacts, the simulation (red dashed line) underestimates the measured signal (green solid line). The overestimation in the Hertzian case is known [13], but the underestimation in the EHL case was not previously known. This underestimation becomes even more contradictory when the lubricant layer is taken into account. Instead of having an interface of steel and air, the interface on the upper part of the plate consists of steel and lubricant. This affects the reflection coefficient (8), which decreases due to an increase in density (ρ_2 increases). A change of reflection coefficient was not taking into account by using Hsu's script [17] for Green's function. The amplitude of EHL impacts is not only higher in comparison with the amplitude of the simulated signal (Fig. 7), but also higher in comparison with the amplitude of a Hertzian impact. Figure 8 shows the spectra of the measured signals of both Hertzian impact (yellow dashed line) and EHL impact (green dashed line). Both impacts are caused by a steel ball ($\varnothing$2 mm) dropped from identical height (350 mm) with the paraffin lubricant layer as the only difference. The difference in amplitude indicates a bigger change in momentum for the EHL impacts in comparison with the

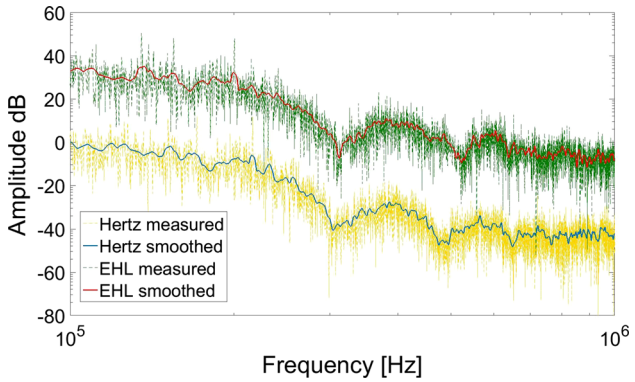

Fig. 8 Comparison of measured spectra of EHL and Hertzian impacts with a ball (RB2 G20) dropped from 350 mm height (Color figure online)

Hertzian impacts, which is in line with higher ball rebounds for Hertzian impacts observed during the tests. However, integration of the force functions suggest otherwise. While the impulse for the EHL impact (RB2 G20 and 350 mm drop height) is $-151.4 * 10^{-6}$ N s, the integration of the Hertzian force results in $-173.9 * 10^{-6}$ N s.

$$\mathrm{RC} = \frac{Z_2 - Z_1}{Z_2 + Z_1} = \frac{c_{p2}\rho_2 - c_{p1}\rho_1}{c_{p2}\rho_2 + c_{p1}\rho_1} \tag{8}$$

While amplitudes deviate between simulation and measurement, the effect of covering third- and higher-order zero frequencies predicted by the simulation is also observed for measured signals (Fig. 7). The position of the zero frequencies, however, does differ between simulated and measured signals. Instead of a shift towards lower frequencies, as suggested by the simulation (Fig. 5), zero frequencies of an EHL impact shift towards higher frequencies when compared to the Hertzian reference impact (Fig. 8). Therefore, a moving average of 50 measurements points in the frequency domain (blue and red line in Fig. 8) was used to identify the position of the zero frequencies within the noisy measurements.

This shift of zero frequencies is even more apparent in Fig. 9 where normalized zero frequencies for all test conditions of the infinite plate are shown. All frequencies, of both Hertzian impact and EHL impacts, are normalized by multiplication with the contact time t_c of the Hertzian reference case. The error bars represent the standard deviation for the four and the eight repetitions of Hertzian and EHL measurements, respectively. The transparent marker represents the Hertzian reference measurements. As found in McLaskey and Glaser [13], normalized zero frequencies of Hertzian reference measurements fit Reed's [19] contact model well ($f_{\mathrm{Zero},1} = 1.75$ and $f_{\mathrm{Zero},2} = 2.75$). EHL impacts (markers with solid fill) in comparison are without exception at higher normalized zero frequencies. The deviation between different test conditions (ball size

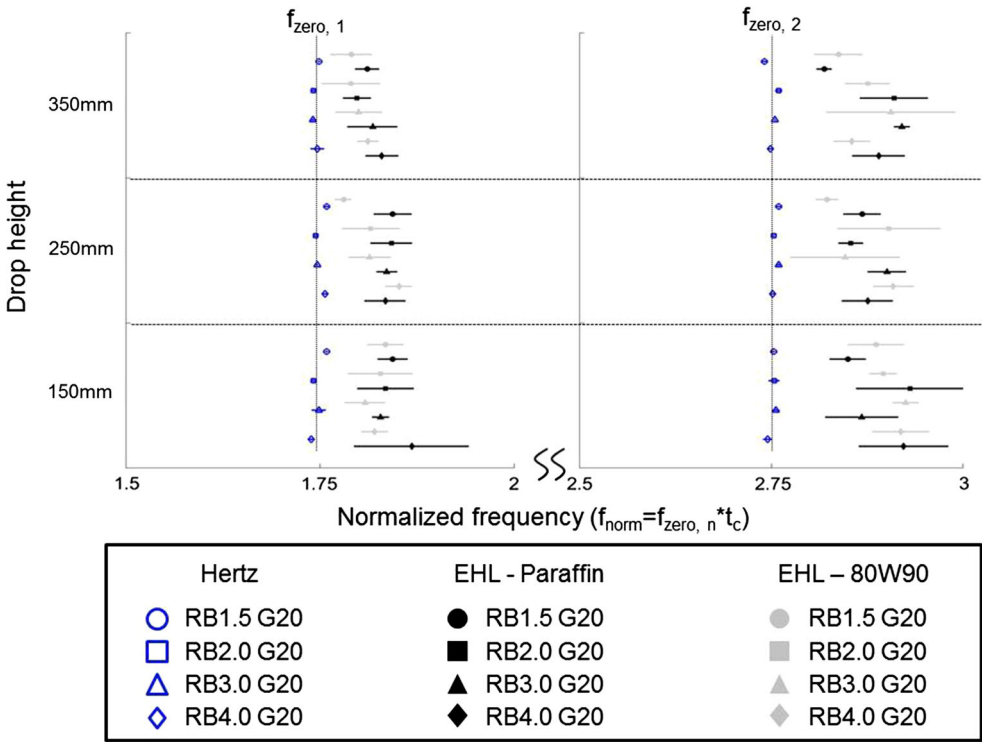

Fig. 9 Zero frequencies of first and second order normalized to the Hertzian reference contact time for different drop heights and ball sizes

and drop height) as well as between repetitions is larger than for the Hertzian reference measurements. This is most probably a result of the way in which the lubricant layer is prepared, because any deviation in initial film thickness is expected to influence the zero frequencies by influencing impact velocity. A significant difference between the lubricants used could, however, not be observed, even though signals of EHL impacts with the lubricant 80W90 (grey marker) tend to have lower normalized frequencies as EHL impacts with paraffin (black marker) especially for the first zero frequency.

Both amplitude and the shift of zero frequencies behave in a contradictory manner when comparing simulations and measurements. The difference in amplitude could be caused by the lubricant layer acting as a couplant during excitation. However, this is not an explanation for the mismatch of zero frequencies. Another approach to provide an explanation of the difference between simulated and measured spectra could be solidification of the lubricant layer and the nature of the EHL contact itself. As Fig. 10 shows, the elastic deformations are substantially different as regards an EHL and a Hertzian impact. Note must also be taken that the y-axis in Fig. 10 is not to scale and deformations therefore are highly emphasized, in order to show basic differences with and without lubricant. While the Hertzian impact (Fig. 10a) results in a uniform deformation of both plate and ball, the EHL impact (Fig. 10b) results in a deformation that is more localized due to the partly solidified lubricant (indicated by the colour scheme). Furthermore, the

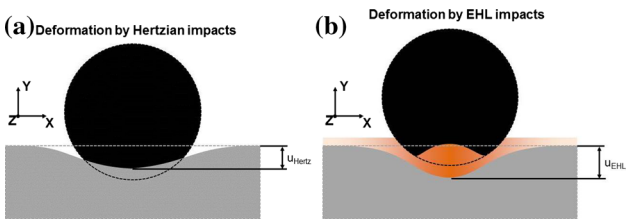

Fig. 10 Schematic drawing of deformation during a Hertzian impact and an EHL impact. EHL deformation is based on Simulations of Larsson and Höglund [18]. Please notice the deformation is exaggerated for visualization purposes. **a** Hertzian impact. **b** EHL impact

maximum deformation is larger in the EHL case compared to Hertzian impact for the center position, as was previously observed by Larsson and Höglund [18].

Simulations in this investigation, are based on a point assumption. A global force function is applied at a single point assuming the contact area is so small that it can be considered to be a single point. However, this assumption also implies that deformations within the contact area are uniform so that the global force function may be used, which might be true for the Hertzian impact, but is definitely violated by the EHL impact. The difference on a local scale could be the cause of both amplitude (higher maximum deformation for EHL impacts) and frequency shift (localized faster deformation changes). A possible solution for future investigations could be to use the Green's function approach to transfer deformations within the system instead of global forces coupled to deformations by fully elastic models.

4.2 Boundary Restricted System

A previous study [16] showed that an elastic wave excited by Hertzian contacts in boundary restricted systems reduces to a resonance problem once wave and source interact. As Fig. 11 shows the difference in excitation force between EHL impact and Hertz impact does not influence the measured signal. With both excitations, identical resonances are triggered and the spectra are almost identical, except for an additional spike in between resonances for the Hertzian excitation.

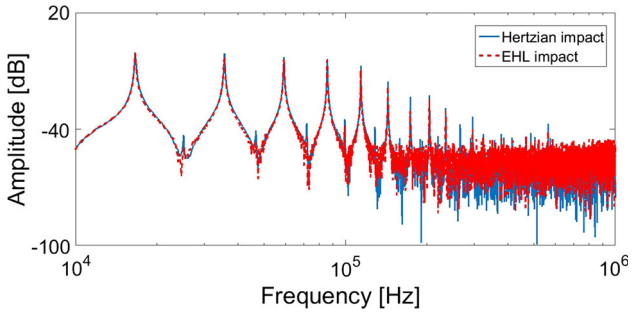

Fig. 11 Comparison of resonances in the boundary restricted system for Hertzian and EHL impacts of a ball (RB4 G20) dropped from 350 mm height

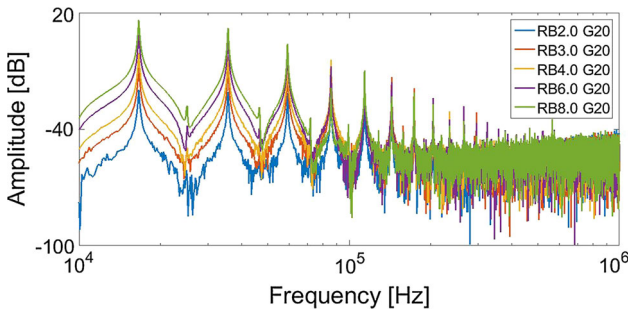

Fig. 12 Comparison of resonances in the boundary restricted system EHL impacts with different ball sizes dropped from 350 mm height

A change in impact energy by changing ball size only influenced the amplitudes (Fig. 12) of the resonances, which is also in line with previous Hertzian investigations [16]. However, a change in ball size does influence the resonance cut-off, due to the change of contact time. For Hertzian impact, the −20dB cut-off and the first zero frequency agree to a high extent [16]. In the case of EHL impacts, it was found that resonance cut-offs occur much earlier. As Fig. 13 shows the Hertzian contact (blue dashed line) excites to a higher degree higher resonances in comparison with an EHL contact (red solid line). A reason for the earlier cut-off could be the damping of the EHL film when compared with the dry Hertzian impact.

5 Summary

In this study, a simulated spectrum, based on a Green's function approach and excited by an EHL contact, is presented. The simulated spectrum partly showed good agreement with measured elastic waves. The overall shape of the spectrum and a covering of zero frequencies of higher order (3rd order and higher), most probably due to

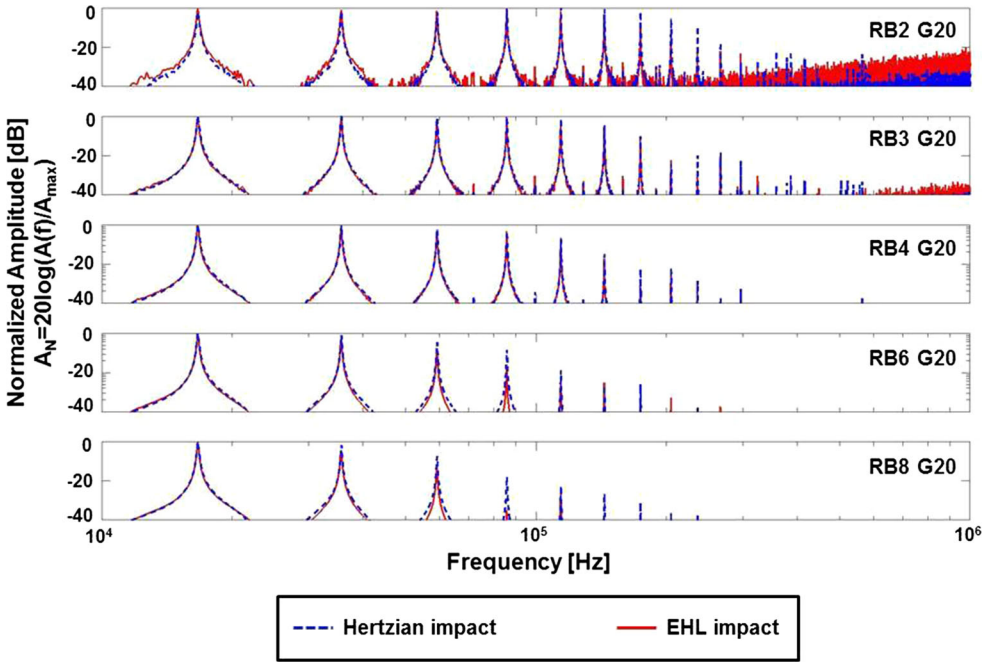

Fig. 13 Comparison of normalized spectra of signals excited by Hertzian and EHL impacts (Color figure online)

cavitation, was observed on both measured and simulated spectra. However, the zero frequencies of simulation and measurement do not match. This could be caused by the point assumption used in the Green's function approach. It is, therefore, suggested that in future investigations of EHL contacts a Green's function approach based on deformation rather than on global force be used. The measured normalized zero frequencies were found to be higher for EHL excited elastic waves than for those excited by a Hertzian contact. A significant differentiation of normalized zero frequencies due to different lubricants could not be observed, due to relative large deviations between repetitions, but the lubricant with higher viscosity tended to have lower normalized first zero frequencies. Additionally, it was observed that boundary restricted systems excited by EHL impacts resulted in the same resonance behaviour as for Hertzian excited systems. The only observed difference was a damping of resonances at higher frequencies, which is most likely caused by the lubrication film.

Acknowledgements The authors would like to acknowledge the financial support of SKF and VINNOVA, as well as the helpful discussions with SKF-researchers, among them Dr. Florin Tatar, SKF-ERC, Netherlands.

References

1. Miettinen, J., Andersson, P.: Acoustic emission of rolling bearings lubricated with contaminated grease. Tribol. Int. **33**(11), 777–787 (2000)
2. Tandon, N., Ramakrishna, K.M., Yadava, G.S.: Condition monitoring of electric motor ball bearings for the detection of grease contaminants. Tribol. Int. **40**(1), 29–36 (2007)
3. Akagaki, T., Nakamura, M., Monzen, T., Kawabata, M.: Analysis of the behaviour of rolling bearings in contaminated oil using some condition monitoring techniques. Proc. Inst. Mech. Eng. Part J J. Eng. Tribol. **220**(5), 447–453 (2006)
4. Miettinen, J., Pataniitty, P.: Acoustic emission in monitoring extremely slowly rotating rolling bearing. In: McIntyre, J., Sleeman, D. (eds.) COMADEM '99, Proceedings, pp. 289–297, 1999. 12th International Congress on Condition Monitoring and Diagnostic Engineering Management, UNIV Sunderland, Sunderland, England, 7–9 July 1999
5. Schnabel, S., Marklund, P., Larsson, R.: Study of the short-term effect of Fe_3O_4 particles in rolling element bearings: observation of vibration, friction and change of surface topography of contaminated angular contact ball bearings. Proc. Inst. Mech. Eng. Part J J. Eng. Tribol. **228**(10), 1063–1070 (2014)
6. Miettinen, J., Andersson, P., Wikström, V.: Analysis of grease lubrication of a ball bearing using acoustic emission measurement. Proc. Inst. Mech. Eng. Part J J. Eng. Tribol. **215**(6), 535–544 (2001)
7. Niknam, S.A., Songmene, V., Joe Au, Y.H.: The use of acoustic emission information to distinguish between dry and lubricated rolling element bearings in low-speed rotating machines. Int. J. Adv. Manuf. Technol. **69**(9–12), 2679–2689 (2013)
8. He, Y., Zhang, X., Friswell, M.I.: Defect diagnosis for rolling element bearings using acoustic emission. J. Vib. Acoust. Trans. ASME **131**(6), 061012 (2009)
9. Elforjani, M., Mba, D.: Accelerated natural fault diagnosis in slow speed bearings with acoustic emission. Eng. Fract. Mech. **77**(1), 112–127 (2010)
10. Hamel, M., Addali, A., Mba, D.: Monitoring oil film regimes with acoustic emission. Proc. Inst. Mech. Eng. Part J J. Eng. Tribol. **228**(2), 223–231 (2014)
11. Rahman, Z., Ohba, H., Yoshioka, T., Yamamoto, T.: Incipient damage detection and its propagation monitoring of rolling contact fatigue by acoustic emission. Tribol. Int. **42**(6), 807–815 (2009)
12. Wang, L., Wood, R., Sun, J.: Acoustic emissions from oil lubricated metal on metal sliding contacts. Insight **50**(9), 506–511 (2008)
13. McLaskey, G.C., Glaser, S.D.: Hertzian impact: experimental study of the force pulse and resulting stress waves. J. Acoust. Soc. Am. **128**(3), 1087–1096 (2010)
14. Zhong, P., Tong, H.L., Cocks, F.H., Pearle, M.S., Preminger, G.M.: Transient cavitation and acoustic emission produced by different laser lithotripters. J. Endourol. **12**(4), 371–378 (1998)
15. McLaskey, G.C., Glaser, S.D.: Acoustic emission sensor calibration for absolute source measurements. J. Nondestr. Eval. **31**(2), 157–168 (2012)
16. Schnabel, S., Golling, S., Marklund, P., Larsson, R.: Absolute measurement of elastic waves excited by Hertzian contacts in boundary restricted systems. Tribol. Lett. (submitted)
17. Hsu, N.: Dynamic green's functions of an infinite plate—a computer program. Technical Report No. NBSIR 85-3234, National Bureau of Standards, Center of Manufacturing Engineering, Gaithersburg (1985)
18. Larsson, R., Höglund, E.: Numerical simulation of a ball impacting and rebounding a lubricated surface. J. Tribol. **117**(1), 94–102 (1995)
19. Reed, J.: Energy losses due to elastic wave propagation during an elastic impact. J. Phys. D Appl. Phys. **18**, 2329–2337 (1985)